

# SAM-aware Test-time Adaptation for Universal Medical Image Segmentation

Jianghao Wu<sup>1,2</sup> Yicheng Wu<sup>1†</sup> Yutong Xie<sup>2</sup> Wenjia Bai<sup>3</sup> You Zhang<sup>4</sup>

Feilong Tang<sup>1,2</sup> Yulong Li<sup>2</sup> Yasmeen George<sup>1</sup> Imran Razzak<sup>2</sup>

<sup>1</sup>Monash University <sup>2</sup>Mohamed bin Zayed University of Artificial Intelligence

<sup>3</sup>Imperial College London <sup>4</sup>UT Southwestern Medical Center

## Abstract

Universal medical image segmentation using the Segment Anything Model (SAM) remains challenging due to its limited adaptability to medical domains. Existing adaptations, such as MedSAM, enhance SAM’s performance in medical imaging but at the cost of reduced generalization to unseen data. Therefore, in this paper, we propose SAM-aware Test-Time Adaptation (SAM-TTA), a fundamentally different pipeline that preserves the generalization of SAM while improving its segmentation performance in medical imaging via a test-time framework. SAM-TTA tackles two key challenges: (1) input-level discrepancies caused by differences in image acquisition between natural and medical images and (2) semantic-level discrepancies due to fundamental differences in object definition between natural and medical domains (e.g., clear boundaries vs. ambiguous structures). Specifically, our SAM-TTA framework comprises (1) Self-adaptive Bezier Curve-based Transformation (SBCT), which adaptively converts single-channel medical images into three-channel SAM-compatible inputs while maintaining structural integrity, to mitigate the input gap between medical and natural images, and (2) Dual-scale Uncertainty-driven Mean Teacher adaptation (DUMT), which employs consistency learning to align SAM’s internal representations to medical semantics, enabling efficient adaptation without auxiliary supervision or expensive retraining. Extensive experiments on five public datasets demonstrate that our SAM-TTA outperforms existing TTA approaches and even surpasses fully fine-tuned models such as MedSAM in certain scenarios, establishing a new paradigm for universal medical image segmentation. Code can be found at <https://github.com/JianghaoWu/SAM-TTA>.

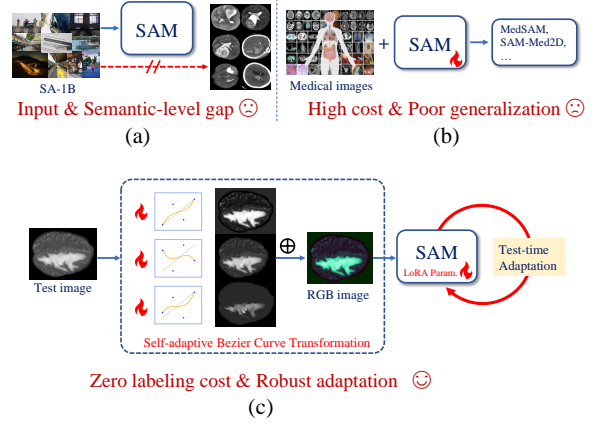


Figure 1. **Overview of challenges in adapting SAM to medical image segmentation.** (a) The input-level and semantic-level domain gaps between the large-scale SA-1B dataset and medical images lead to inferior segmentation performance. (b) Fine-tuning-based approaches (e.g., MedSAM) require costly training and lead to poor generalization. (c) Our self-adaptive Bezier curve-based test-time adaptation achieves zero labeling cost and robust adaptation without large-scale re-training.

## 1. Introduction

Segment Anything Model (SAM) [21] has demonstrated remarkable capabilities in image segmentation across diverse tasks [4, 16]. By leveraging a large-scale, diverse dataset (i.e., SA-1B), SAM exhibits exceptional zero-shot generalization, enabling it to segment unseen objects and domains effectively [46]. This makes SAM a promising foundation model with broad downstream applications [44], including medical image segmentation [48], where high-quality segmentation is critical for clinical decision-making. However, despite its potential, SAM struggles to meet the stringent accuracy and robustness requirements necessary for clinical deployment in medical image segmentation [41].

One main reason lies in the discrepancies at the input level and the semantic level [48]. As seen in Figure 1 (a), differences in acquisition protocols, imaging devices, and patient populations introduce a substantial distribution

<sup>†</sup>Correspondence to yicheng.wu@monash.edu.

shift between natural images (*e.g.*, SA-1B) and real-world clinical data. This includes the mismatch of input channels, as SAM is designed for three-channel RGB images, whereas most medical scans (*e.g.*, CT, MRI) are single-channel grayscale maps. Moreover, semantic-level discrepancies stem from the fundamental differences between natural and medical segmentation tasks. Medical segmentation often requires delineating ambiguous, low-contrast boundaries and a contextual understanding of anatomical structures (*e.g.*, organs and tumors) [24, 42], which contrasts with the clear object boundaries found in natural images. Without proper adaptation, SAM remains challenging to align with these tasks, leading to sub-optimal performance for universal medical image segmentation.

To address this issue, several studies have explored fine-tuning SAM on large-scale medical datasets (*e.g.*, MedSAM [28]), shown in Figure 1 (b). However, there are two obstacles to large-scale fine-tuning: **High computational cost**: Fine-tuning large models like SAM demands substantial computational resources and extensive annotated medical data, which may be impractical for local clinical institutions with limited infrastructure. **Reduced generalization**: Fine-tuning on a specific medical dataset often leads to catastrophic forgetting, significantly impairing the model’s ability to generalize to unseen test images, particularly in the presence of distribution shifts and diverse medical imaging conditions [9, 25]. Therefore, an alternative approach is highly desirable to enable SAM to adapt effectively to new medical images without relying on large-scale fine-tuning.

Therefore, we propose SAM-aware Test-Time Adaptation (SAM-TTA) illustrated in Figure 1(c), a framework that enables unsupervised adaptation to unseen medical images without task-specific fine-tuning. To address input-level discrepancies, particularly the input channel mismatch, a common approach is to replicate grayscale images across three channels [12, 28]. However, this fails to capture essential medical image features for segmentation. Instead, we introduce a self-adaptive Bezier curve-based grayscale transformation, an efficient operation that converts grayscale medical images into three-channel inputs compatible with SAM. Unlike generative approaches such as GANs [5] and diffusion models [20], which require extensive training and are often impractical at test time, our method optimizes only a few parameters, adapting the input while preserving SAM’s original representations. Beyond input-level discrepancies, we further tackle semantic-level discrepancies by introducing a dual-scale uncertainty-driven Mean Teacher adaptation, which refines a small subset of parameters during inference. Leveraging SAM’s IoU score for uncertainty estimation and dual-scale segmentation masks, our SAM-TTA model effectively minimizes uncertainty and enforces dual-scale consistency for improved test-time adaptation. Extensive experiments demonstrate

that SAM-TTA achieves state-of-the-art test-time performance without costly retraining or the need for large-scale training data in universal medical image segmentation.

Overall, our main contributions are as follows:

- We propose SAM-TTA, a new paradigm that efficiently adapts the powerful SAM to medical images by addressing both input-level and semantic-level discrepancies without extensive retraining.
- We introduce a novel self-adaptive Bezier curve-based grayscale transformation, which optimizes only a small number of parameters at test time, aligning medical images with SAM’s expected input domain while preserving its pre-trained knowledge.
- We demonstrate the effectiveness of our SAM-TTA in improving SAM’s segmentation performance across five medical image datasets, achieving significant improvements in test-time adaptation.
- Our SAM-TTA can be seamlessly integrated into existing fine-tuned models, such as MedSAM, to further boost their performance in medical image segmentation.

## 2. Related Work

**Foundation Models for Image Segmentation.** Deep learning models pre-trained on large-scale datasets have significantly advanced computer vision tasks such as semantic segmentation, achieving state-of-the-art performance on benchmarks like Pascal VOC [11] and COCO [27]. However, these models typically struggle in zero-shot or few-shot scenarios. Recently, vision foundation models (FMs) such as CLIP [31], DINO [30], and especially the SAM [21], trained on extensive web-scale data, have opened new possibilities for generalizable segmentation [2, 47]. SAM offers powerful zero-shot segmentation capabilities through flexible prompts, including points, boxes, masks, and text. Its broad applicability has spurred extensive research into its performance on challenging medical image segmentation tasks [7]. MedSAM [28] is one of the first comprehensive attempts to fine-tune SAM for medical images on a large-scale dataset while preserving its box-prompt functionality. SAM-Med2D [8] builds on this approach by fine-tuning SAM’s entire architecture on 4.6 million medical images, making it the largest medical adaptation of SAM to date. The Medical SAM Adapter (MedSA) [41] introduces a lightweight adapter with specialized modules such as SD-Trans and HyP-Adpt for multimodal segmentation. For volumetric data, MA-SAM [3] proposes modality-agnostic 3D adapters in the image encoder to facilitate segmentation across CT, MRI, and surgical video modalities by integrating volumetric and temporal information. Moreover, MedCLIP-SAM [22] leverages CLIP’s text encoder for text-driven segmentation tasks, such as segmenting the left ventricle. Nevertheless, most SAM adaptations rely on large-scale annotations or full fine-tuning,

which is impractical under significant domain shifts. In contrast, our work focuses on unsupervised test-time adaptation to reduce the dependency on labeled data while fully leveraging SAM’s generalization capabilities.

**Test Time Adaptation.** Test-Time Adaptation (TTA) adapts the source model using only unlabeled target data at test time, without architectural modifications [34, 38, 43]. It requires on-the-fly updates without multi-epoch fine-tuning [6, 26]. Sun et al. [32] introduced an auxiliary branch for rotation prediction, while Karani et al. [18] proposed a shallow normalization network fine-tuned via a Denoising Auto-Encoder (DAE). However, these methods modify the segmentation model, limiting their applicability to pre-trained foundation models like SAM [21]. Fully TTA operates without access to training data or auxiliary supervision [29, 35]. PTBN [29] and TENT [35] use batch normalization to adapt feature distributions, while WCEM [23] and SAR [37] improve stability by filtering unreliable predictions. UPL-TTA [40] generates pseudo-labels through weak augmentations, dropout, and multi-decoder ensembles to enhance adaptation. CoTTA [36] stabilizes continual test-time adaptation by applying teacher model updates with stochastic weight averaging and augmenting pseudo-label consistency. However, these methods focus only on refining model predictions without adjusting input representations. When the domain gap is large, they struggle to align test images with the source model’s distribution, limiting adaptation performance. In contrast, our method tackles this issue by transforming test-time inputs via self-adaptive grayscale intensity normalization, enhancing alignment with SAM’s learned features and enabling more effective adaptation across diverse medical domains.

### 3. Method

In this work, we introduce SAM-TTA, a novel SAM-aware test-time adaptation framework for universal medical image segmentation. As shown in Figure 2, our framework comprises two main components (1) self-adaptive Bezier curve-based grayscale transformation for input-level gap caused by differences in image acquisition between natural and medical domains, and (2) dual-scale uncertainty-driven Mean Teacher adaptation for semantic-level discrepancies due to the distinct nature of medical and natural image segmentation tasks.

#### 3.1. Overview of Segment Anything Model

SAM, denoted by  $F$ , consists of three primary modules. First, the image encoder,  $z = f(X)$ , extracts feature representations from the input image  $X$  and is pre-trained using a masked autoencoder (MAE) [14]. Second, the prompt encoder,  $e = g(p)$ , encodes user-provided prompts  $p$  to guide segmentation. Third, the mask decoder,  $h(z, e)$ , fuses the image and prompt features to generate segmentation masks.

After pre-training the image encoder, SAM is fine-tuned on the large-scale SA-1B dataset [21], which contains 1.1 billion labeled masks, using a combination of focal loss and Dice loss. During inference, the image encoder first processes a test image  $X$  to produce feature representations  $z = f(X)$ . Then, given encoded prompts  $e$ , the mask decoder produces three outputs: a coarse low-resolution mask  $M_l$ , a refined high-resolution mask  $M_h$ , and a confidence IoU score  $S_{\text{IoU}}$  estimating segmentation quality.

#### 3.2. Self-adaptive Grayscale Transformation

In medical image segmentation, simply replicating the grayscale channel or using generative models to synthesize three-channel inputs fails to adequately capture the distinct intensity and structural characteristics of modalities like CT and MRI. Traditional Bezier curve-based nonlinear transformations [49] offer a versatile framework for intensity mapping. However, they rely on manually selected control points, a process that is both labor-intensive and often suboptimal since fixed mappings may not generalize well across diverse imaging modalities.

To overcome these limitations, we propose a Self-adaptive Bezier Curve-based grayscale Transformation (SBCT) that dynamically learns optimal intensity mappings at test time for each channel. SBCT leverages a cubic Bezier curve defined as

$$B(t) = (1-t)^3 P_0 + 3t(1-t)^2 P_1 + 3t^2(1-t) P_2 + t^3 P_3, \quad (1)$$

where  $t \in [0, 1]$  represents the normalized pixel intensity and  $B(t)$  denotes the transformed intensity. To ensure numerical stability and prevent degenerate mappings, the  $x$ -coordinates of the control points are fixed at  $[0, 0.33, 0.66, 1.0]$ , while the  $y$ -coordinates are parameterized as learnable variables

$$P_j = \sigma(\theta_j), \quad j = 0, 1, 2, 3, \quad (2)$$

with  $\theta_j$  being unconstrained parameters and  $\sigma$  the sigmoid function that constrains  $P_j$  within  $[0, 1]$ .

Given a grayscale test image  $X \in \mathbb{R}^{1 \times H \times W}$ , we construct a three-channel representation applying three independent SBCTs. Specifically, for each pixel  $(h, w)$  in  $X$ , the  $i$ -th channel is computed as

$$X^i(h, w) = B(X(h, w); P^i), \quad i = 1, 2, 3, \quad (3)$$

where  $P^i = \{P_0^i, P_1^i, P_2^i, P_3^i\}$  are the learnable parameters associated with the  $i$ -th transformation. The final three-channel image is then obtained by concatenating these channels

$$\hat{X} = \text{concat}(X^1, X^2, X^3) \in \mathbb{R}^{3 \times H \times W}, \quad (4)$$

note that for an RGB test image,  $X^1, X^2, X^3$  are obtained by applying SBCT independently to each of the original R, G, and B channels.

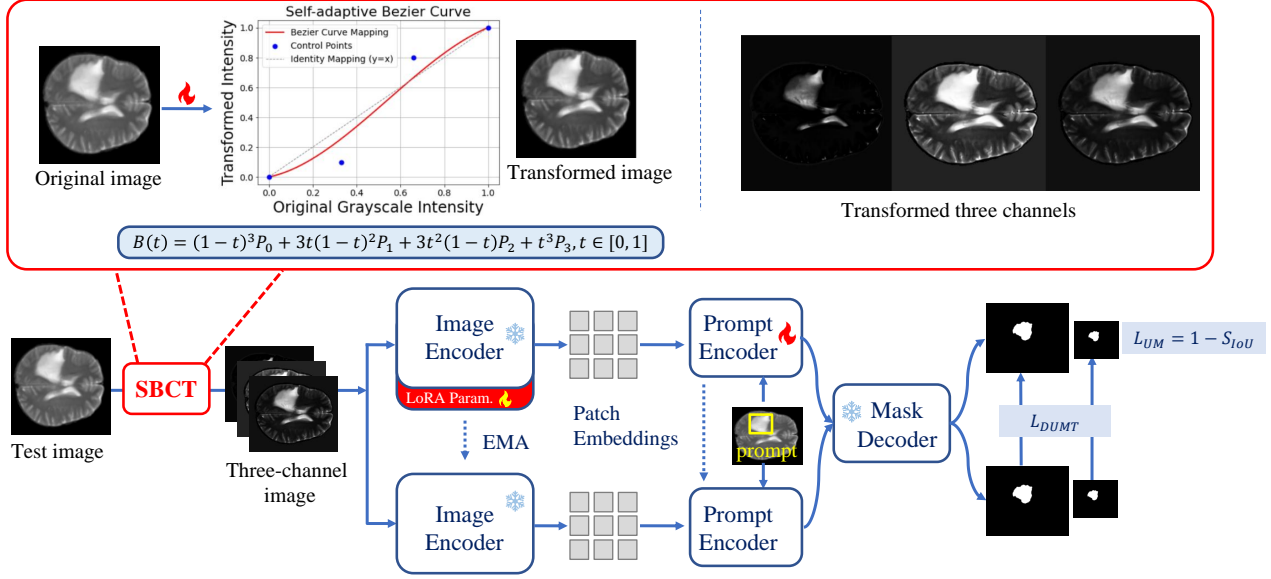


Figure 2. **Overview of our proposed framework.** SBCT converts a grayscale medical image into a three-channel representation. The resulting image is fed into SAM, where a dual-scale uncertainty-driven mean teacher updates the student model via LoRA using a dual-scale, uncertainty-weighted Dice loss ( $L_{DUMT}$ ) and an IoU-driven uncertainty minimization loss ( $L_{UM}$ ). The teacher model is updated via exponential moving average (EMA) for robust unsupervised adaptation.

The transformed image  $\hat{X}$  is fed into SAM to obtain the image embedding  $\hat{z} = f(\hat{X})$ . With the corresponding prompt, SAM produces a low-resolution mask  $\hat{M}_l$ , a high-resolution mask  $\hat{M}_h$ , and a confidence IoU score  $S_{IoU}$ .

The confidence IoU score  $S_{IoU}$  provides an intrinsic estimation of segmentation quality, serving as a self-supervised uncertainty metric. We introduce an uncertainty reduction loss that encourages SAM to refine its segmentation by maximizing its predicted confidence score defined as

$$\mathcal{L}_{UM} = 1 - S_{IoU}, \quad (5)$$

where  $S_{IoU}$  is computed internally by SAM. Note that this loss is not derived from any ground truth labels but is solely designed to reduce prediction uncertainty.

### 3.3. Dual-scale Uncertainty-Driven Adaptation

While SBCT converts single-channel medical images into three-channel inputs for SAM, a semantic gap persists. Since SAM is pre-trained on natural images, its representations are tuned for natural scenes rather than the distinct anatomical structures and modality-specific patterns of medical images. As a result, SBCT alone cannot fully adapt SAM’s features to the medical domain, which limits segmentation performance. To overcome this semantic misalignment without relying on ground-truth annotations, we propose Dual-scale Uncertainty-driven Mean Teacher adaptation (DUMT). This approach leverages two inherent self-supervisory signals provided by SAM: (a) a predicted IoU score that acts as an uncertainty estimate to priori-

tize more reliable predictions, and (b) dual-scale segmentation outputs (low-resolution and high-resolution masks) that enforce consistency across spatial scales. These self-supervised signals enable SAM to refine its segmentation representations while ensuring stable adaptation to the medical domain.

We adopt a mean-teacher framework for unsupervised adaptation, where both the student model  $F^S$  and teacher model  $F^T$  are initialized with SAM’s pre-trained weights. To enable efficient adaptation, we integrate Low-Rank Adaptation (LoRA) [15] into the image encoder of  $F^S$ , updating only a small subset of parameters, while keeping the prompt encoder trainable to dynamically adjust to the input. The mask decoder remains frozen to preserve its ability to estimate segmentation quality via the IoU score and prevent overfitting to higher IoU values without meaningful segmentation improvement. All supervisory signals for adaptation are obtained from a single forward pass, ensuring computational efficiency while aligning SAM’s semantic representations with the medical domain.

During adaptation, we enforce consistency between the student and teacher predictions across multiple scales. We impose a dual-scale consistency constraint based on Dice loss, ensuring that the adaptation process aligns both coarse and fine-grained segmentations. The student’s predicted IoU score  $S_{IoU}$  is employed as an uncertainty measure, and the loss is weighted by  $S_{IoU}^3$  to amplify the importance of more reliable predictions. The dual-scale uncertainty-



weighted Dice loss is expressed as

$$\mathcal{L}_{\text{DUMT}} = \frac{1}{2} \left( \frac{2 \cdot \hat{M}_h^S \cdot \hat{M}_h^T}{\hat{M}_h^S + \hat{M}_h^T} + \frac{2 \cdot \hat{M}_l^S \cdot \hat{M}_l^T}{\hat{M}_l^S + \hat{M}_l^T} \right) \cdot S_{\text{IoU}}^3. \quad (6)$$

The overall test time optimization objective for the SBCT and the student model is defined as

$$\mathcal{L}_{\text{TTA}} = \mathcal{L}_{\text{DUMT}} + \mathcal{L}_{\text{UM}}, \quad (7)$$

while the teacher model is updated via an Exponential Moving Average (EMA) of the student’s weights, providing a smoother supervisory signal over successive iterations.

Test-time adaptation is executed sequentially for each test image, as illustrated in Algorithm 1. For a given test image  $X$ , SBCT first transforms the grayscale image into a three-channel representation  $\hat{X}$ . Subsequently, the DUMT framework refines the student model by minimizing the adaptation loss  $\mathcal{L}_{\text{TTA}}$ . Once updated, the student model generates the final segmentation output  $\hat{M}_h$  for  $X$ . This procedure is repeated for each subsequent test image.

## 4. Experiments and Results

### 4.1. Experimental Setup

**Backbone.** We adopt ViT-B [10] as the encoder and employ the standard prompt and mask encoders from SAM. We evaluate our proposed method using bounding box prompts. **Competing Methods.** We evaluate multiple test-time adaptation approaches and one SAM-based source-free domain adaptation method. In our evaluations, direct testing of the pre-trained SAM (SAM) is used as the baseline. **TENT** [35] that updates the parameters by minimizing the entropy of model predictions on new test data; **MT** [33] that utilizes a teacher-student structure for adaptation; **CoTTA** [36] that employs test-time augmentation-based pseudo labels for adaptation; **UPL-TTA** [40] that introduces a weak transformation and a multi-decoder to generate reliable pseudo labels and diverse predictions for adaptation; **WeSAM** [45] that uses a self-training architecture with anchor network regularization and contrastive loss regularization for source-free SAM adaptation. We also compared our method with two larger-scale medical fine-tuned SAM models: **SAM-Med2D**[8], which uses adapter layers to fine-tune SAM on extensive medical images, and **MedSAM**[28], which fine-tunes SAM’s image encoder and mask decoder on a large annotated medical dataset.

**Datasets.** We evaluate the generalization capability of our proposed method on five distinct medical image segmentation tasks spanning multiple imaging modalities and anatomical structures. Specifically, as shown in Table 1, we consider: (1) **Brain Hemorrhage Segmentation:** The MBH-Seg challenge dataset [39], which comprises non-contrast CT images for segmenting subdural hemorrhage

---

### Algorithm 1: SAM-aware Test-time Adaptation

---

**Input:** Test dataset  $\mathcal{D} = \{X_i\}_{i=1}^N$ , pre-trained SAM model  $F$ , SBCT transformation  $B$ , prompt  $p$ , optimizer, EMA decay  $\alpha$

**Output:** Adapted student model  $F^S$  and segmentation predictions  $\{\hat{M}_h^{(i)}\}_{i=1}^N$

```

1 Initialize  $F^S = F^T = F$ ;
2 for each test image  $X \in \mathcal{D}$  do
3   Compute three-channel representation:  $\hat{X} =$ 
   concat( $B(X; P^1), B(X; P^2), B(X; P^3)$ );
4    $(\hat{M}_l^S, \hat{M}_h^S, S_{\text{IoU}}) \leftarrow F^S(\hat{X}, p)$ ;
5    $(\hat{M}_l^T, \hat{M}_h^T) \leftarrow F^T(\hat{X}, p)$ ;
6
    $\mathcal{L}_{\text{DUMT}} \leftarrow \frac{1}{2} \left( \frac{2 \hat{M}_h^S \cdot \hat{M}_h^T}{\hat{M}_h^S + \hat{M}_h^T} + \frac{2 \hat{M}_l^S \cdot \hat{M}_l^T}{\hat{M}_l^S + \hat{M}_l^T} \right) \cdot S_{\text{IoU}}^3$ 

    $\mathcal{L}_{\text{UM}} \leftarrow 1 - S_{\text{IoU}}$ ;
7    $\mathcal{L}_{\text{TTA}} \leftarrow \mathcal{L}_{\text{DUMT}} + \mathcal{L}_{\text{UM}}$ ;
8   optimizer.zero_grad();
9   Backpropagate and update the parameters  $\theta^S$  of
    $F^S$  and the 12 learnable parameters of SBCT
   by minimizing  $\mathcal{L}_{\text{TTA}}$ .
10  for each parameter  $\theta$  in  $F^T$  do
11     $\theta \leftarrow \alpha \theta + (1 - \alpha) \theta^S$ 
12  end
13   $\hat{M}_h \leftarrow F^S(\hat{X}, p)$ ;
14  Save prediction  $\hat{M}_h$  for image  $X$ ;
15 end
16 return Adapted student model  $F^S$  and predictions
     $\{\hat{M}_h\}_{i=1}^N$ ;
```

---

Table 1. Datasets and the number of test images used in this work.

Dataset	Modality	Testing Samples
MBH-Seg [39]	NCCT	392
BraTS-SSA [1]	T2W / T2F	2165
BraTS-PED [19]	T2W / T2F	1554
CVC-ColonDB [13]	Endoscopic	266
Kvasir-SEG [17]	Endoscopic	700

regions. (2) **Brain Tumor Segmentation:** Two subsets from the BraTS2023 challenge are used for brain tumor segmentation: (a) **BraTS-SSA:** The Sub-Sahara Africa adult glioma dataset [1], evaluated on T2-weighted (T2W) and T2 FLAIR (T2F) modalities; (b) **BraTS-PED:** The pediatric brain tumor dataset [19], also evaluated on T2W and T2F modalities. (3) **Polyp Segmentation:** Two RGB endoscopic datasets are used for polyp segmentation: (a) **CVC-ColonDB:** An RGB dataset [13]; (b) **Kvasir-SEG:** Another RGB dataset [17].

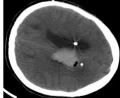








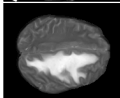








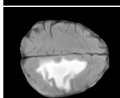








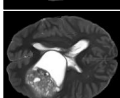

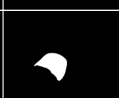
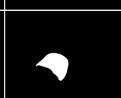
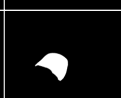
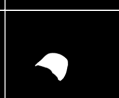
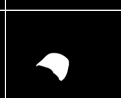
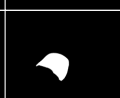

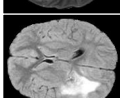








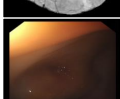

















MBH-Seg									
BraTS-SSA T2W									
BraTS-SSA T2F									
BraTS-PED T2W									
BraTS-PED T2F									
CVC-ColonDB									
Kvasir-SEG									
	Image	Label	SAM	TENT	CoTTA	MT	UPL-TTA	WESAM	SAM-TTA (Ours)

Figure 3. Visual comparison of segmentation results across multiple medical image datasets.

**Evaluation Metrics:** We report Dice Score (DSC) and 95th percentile Hausdorff Distance (HD95) as evaluation metrics. DSC measures the overlap between the predicted and ground-truth segmentation masks, while HD95 evaluates the boundary agreement by computing the 95th percentile of the Hausdorff Distance between them.

**Hyperparameters:** We fine-tune the LoRA module of the ViT-B image encoder and the entire prompt encoder using the Adam optimizer across all experiments. The LoRA module for the image encoder is configured with a low-rank setting of 4. All experiments are conducted on an RTX 3090, with a batch size of 1 per GPU, implemented in PyTorch 2.5.1. The learning rate for the control points of the SBCT is set to 0.01 to enable rapid adaptation, while the learning rate for LoRA and the prompt encoder is 0.001, with a weight decay of 0.0001. Additionally, the EMA rate of the teacher model is set to 0.95.

## 4.2. Quantitative Evaluations

**Adaptation to Brain Hemorrhage Segmentation Task.** To assess the generalization capabilities of SAM and its medically fine-tuned variants, we evaluate on the MBH-Seg challenge dataset [39], published in 2024. This dataset was not used during the fine-tuning of MedSAM [28] or SAM-Med2D [8], providing a completely new test scenario. As shown in Table 2, the original SAM [21] achieves

a DSC of 81.58%, whereas the medical-pretrained MedSAM attains only 80.13%, and SAM-Med2D further drops to 78.95%, indicating a significant generalization gap for these fine-tuned models on unseen medical data. In contrast, other TTA methods yield higher DSC scores ranging from 81.60% to 82.87%, surpassing the baseline SAM and underscoring the promise of test-time adaptation for bridging the domain gap between SAM and medical images. Notably, our proposed SAM-TTA further boosts the DSC to 83.24%. With respect to HD95, although MedSAM outperforms the original SAM, SAM-Med2D still performs worse than SAM; notably, our method achieves the lowest HD95, further confirming its effectiveness.

**Adaptation to Brain Tumor Segmentation Task.** To further validate the effectiveness of our proposed method, we evaluate on the SSA and PED subsets of the BraTS 2023 challenge dataset. Notably, while the original BraTS dataset was used for training MedSAM [28] and SAM-Med2D [8], the BraTS-SSA and BraTS-PED subsets were not, thereby providing the same segmentation task in a distinct testing scenario. As shown in Table 2, the original SAM [21] achieves DSC scores ranging from 78.77% to 85.67%. In contrast, SAM-Med2D performs worse than SAM, while MedSAM attains a slightly higher DSC of 85.11%. Moreover, TENT suffers a significant performance drop, likely due to the larger dataset size and its reliance on entropy

Table 2. Quantitative comparison with other methods on grayscale medical image datasets, including MBH-Seg, BraTS-SSA, and BraTS-PED. Evaluation metrics include DSC (%) and HD95 (pixels). Note that these datasets are not used to train fine-tuned models [8, 28].

Method	MBH-Seg		BraTS-SSA T2W		BraTS-SSA T2F		BraTS-PED T2W		BraTS-PED T2F		Average	
	DSC	HD95	DSC	HD95	DSC	HD95	DSC	HD95	DSC	HD95	DSC	HD95
SAM [21]	81.58	8.33	78.77	25.06	79.77	23.49	83.62	15.71	85.67	13.38	81.88	17.19
TENT [35]	81.60	8.30	49.76	45.00	62.70	30.83	68.50	27.47	65.31	29.13	65.57	28.14
CoTTA [36]	81.68	8.25	79.05	25.02	80.07	23.41	83.65	15.71	85.74	13.31	82.02	17.14
MT [33]	82.87	7.52	81.41	23.87	81.72	23.73	87.97	11.87	88.63	11.04	84.52	15.60
UPL-TTA [40]	82.76	7.31	80.10	26.78	80.28	26.41	87.74	12.36	88.78	10.93	83.93	16.75
WESAM [45]	82.54	7.76	81.75	22.36	80.63	25.33	87.63	12.42	88.35	11.24	84.18	15.82
SAM-TTA (Ours)	<b>83.24</b>	<b>6.92</b>	<b>84.05</b>	<b>18.94</b>	<b>85.57</b>	16.45	<b>89.10</b>	<b>9.88</b>	<b>90.39</b>	8.81	<b>86.47</b>	<b>12.20</b>
SAM-Med2D [8]	78.95	11.47	72.85	32.81	79.32	30.48	77.09	27.70	84.87	23.76	78.61	25.24
MedSAM [28]	80.13	7.79	82.70	19.50	85.33	<b>15.86</b>	87.38	11.70	90.05	<b>8.08</b>	85.11	12.58
MedSAM [28]+Ours	81.75	7.70	85.33	16.53	86.70	14.11	88.95	10.27	90.95	7.11	86.73	11.14

Table 3. Quantitative comparison on RGB medical image datasets (CVC-ColonDB and Kvasir-SEG). Evaluation metrics include DSC (%) and HD95 (pixels). Note that these datasets are used to train fine-tuned models [8, 28].

Method	CVC-ColonDB		Kvasir-SEG	
	DSC	HD95	DSC	HD95
SAM [21]	87.58	8.20	80.95	14.93
TENT [35]	87.68	8.10	82.62	15.58
CoTTA [36]	87.60	8.17	81.01	14.90
MT [33]	87.74	7.96	83.58	13.92
UPL-TTA [40]	87.83	7.98	82.70	13.95
WESAM [45]	87.97	7.95	82.70	13.95
SAM-TTA (Ours)	<b>89.48</b>	<b>6.77</b>	<b>85.34</b>	<b>13.23</b>
SAM-Med2D [8]	90.34	6.57	92.49	8.38
MedSAM [28]	90.27	<u>5.72</u>	89.43	8.49

minimization, which can result in error accumulation and catastrophic forgetting. Other adaptation methods generally yield more stable results, with DSC improvements from 83.93% to 84.52%, except for CoTTA. Our proposed method, however, achieves a DSC of 86.47%, significantly surpassing both the original SAM and MedSAM. In terms of HD95, our approach also attains the lowest score of 12.20, further confirming its superiority.

**Adaptation to Polyp Segmentation Task.** We further evaluate the effectiveness of our proposed method on RGB polyp segmentation datasets. As shown in Table 3, the original SAM [21] achieves DSC scores of 87.58% on the CVC-ColonDB dataset and 80.95% on the Kvasir-SEG dataset, demonstrating acceptable performance on CVC-ColonDB. However, existing TTA methods struggle to improve results on CVC-ColonDB, with the highest DSC reaching only 87.97%. In contrast, fully supervised fine-tuned models such as SAM-Med2D [8] and MedSAM [28], which have been fine-tuned specifically on these datasets, achieve DSC scores of 90.34% and 90.27%, respectively, serving as an upper bound. Our SAM-TTA increases SAM’s

DSC to 89.48% on CVC-ColonDB, approaching this upper bound, and improves DSC on Kvasir-SEG from 80.95% to 85.34%, outperforming existing TTA methods. Moreover, our method achieves the optimal HD95 on both datasets, further confirming its effectiveness.

**Qualitative Visualization.** Figure 3 illustrates qualitative segmentation results on various challenging datasets. For CT images containing rare hemorrhagic lesions (*e.g.*, MBH-Seg), the original SAM misdirects its segmentation towards hyperattenuating artifacts or bright regions, thus neglecting actual lesion boundaries and impairing clinical utility. Existing TTA methods, which heavily depend on refining predictions from the pre-trained SAM, struggle when the initial segmentation disproportionately highlights these irrelevant regions. Similar issues arise in MRI-based BraTS-PED T2W scans, where contrast leakage and lesion-induced hyperintensities similarly mislead the segmentation. Our proposed approach addresses these intensity-induced biases across imaging modalities through adaptive grayscale intensity normalization, enhancing contrast and providing clearer boundary delineation, which leads to substantially improved segmentation accuracy and robustness in clinical scenarios, as shown in Figure 4. Moreover, conventional TTA methods typically accumulate errors during iterative adaptation, increasing the risk of catastrophic forgetting. For instance, on BraTS-SSA and BraTS-PED datasets, certain TTA methods excessively fit their predictions to the provided prompt bounding box, ultimately neglecting the actual target regions. Notably, our method, although primarily designed for grayscale images, also performs robustly on RGB endoscopic images, effectively delineating targets even under blurry conditions.

**Enhancing MedSAM with Our Framework.** We further evaluate the applicability of our method by integrating it into MedSAM, as shown in the last row of Table 2. By incorporating our framework into MedSAM (MedSAM+Ours), we achieve an average DSC of 86.76%

Table 4. Ablation study results on the Brain Tumor Segmentation Dataset. “MT” denotes the use of a mean-teacher framework with LoRA-based updates to the SAM model; “IoU-weighted” indicates that the predicted IoU is used as a weighting factor; and “Dual-Scale” signifies that low-resolution outputs are employed for additional supervision.

Methods					BraTS-SSA T2W		BraTS-SSA T2F		BraTS-PED T2W		BraTS-PED T2F	
SAM	SBCT	MT	IoU-weighted	Dual-Scale	DSC	HD95	DSC	HD95	DSC	HD95	DSC	HD95
✓					78.77	25.06	79.77	23.49	83.62	15.71	85.67	13.38
✓	✓				82.34	20.58	84.16	16.99	87.01	12.85	88.55	10.17
✓	✓	✓			82.46	21.66	84.18	18.37	89.00	10.08	89.51	9.67
✓	✓	✓	✓		83.32	20.36	85.46	16.48	89.05	10.03	90.16	8.90
✓		✓	✓	✓	80.13	26.71	81.84	23.67	88.61	10.81	89.61	9.30
✓	✓	✓	✓	✓	84.05	18.94	85.57	16.45	89.10	9.88	90.39	8.81

and an HD95 of 11.14, outperforming MedSAM alone. These findings demonstrate that our framework is not only effective for adapting SAM but also enhances existing fine-tuned medical segmentation models.

**Computational Efficiency.** Our method outperforms MedSAM by requiring only a single time of optimization per image instead of time-consuming optimizations across numerous images. In addition, while WESAM and UPL-TTA require adaptation times of 0.58s per image and 0.60s per image, respectively, our method takes only 0.364s per image. Given that SAM’s direct inference requires 0.10s per image, our approach incurs an extra 0.26s per image—a modest overhead for the substantial performance gains achieved.

### 4.3. Ablation Study

In this section, we analyze the contribution of each proposed component on the brain tumor segmentation dataset. As shown in Table 4, introducing SBCT significantly improves the DSC, reaching 82.34%, 84.16%, 87.01%, and 88.55% across different settings. This result indicates that simply modifying the input image, without altering the original SAM weights, can yield substantial performance gains.

Furthermore, incorporating a mean-teacher framework with LoRA updates (MT) further boosts both DSC and HD95 relative to SBCT alone, though it only utilizes high-resolution outputs. Adopting IoU-weighted optimization (IoU-weighted) refines the segmentation by leveraging the predicted IoU as a weighting factor. Finally, employing low-resolution outputs for additional supervision (Dual-Scale) consistently provides further improvements.

## 5. Conclusion

In this paper, we have presented a novel unsupervised test-time adaptation framework, SAM-TTA, for the SAM in medical image segmentation. Our SAM-TTA addresses the input-level discrepancies caused by differences in image acquisition between natural and medical domains, and the semantic-level discrepancies arising from the distinct nature of medical and natural image segmentation tasks. We

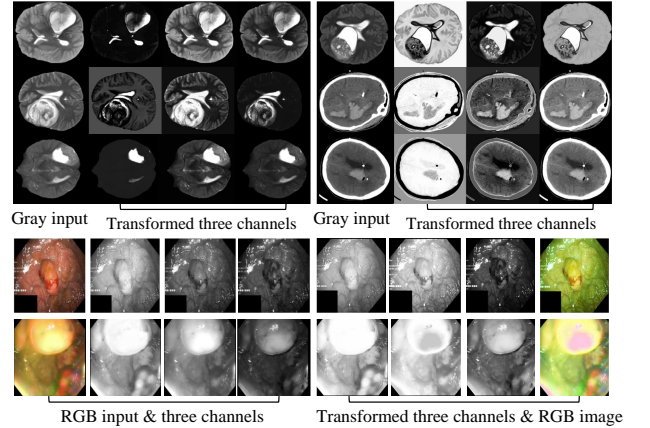


Figure 4. **Visualization of SBCT images across different modalities.** Original grayscale inputs (MRI, CT) and RGB inputs (endoscopy) are presented alongside their SBCT-generated three-channel representations.

first proposed a self-adaptive Bezier curve-based grayscale transformation to convert single-channel medical images into a three-channel representation. Furthermore, by integrating a Mean-Teacher framework with LoRA-based updates and enforcing dual-scale consistency weighted by the predicted IoU score, we enable SAM to refine its internal representations and segmentation predictions in an unsupervised manner. Extensive experiments on five medical imaging datasets demonstrate that our approach significantly improves the segmentation performance of SAM, outperforming existing test-time adaptation methods and even approaching or exceeding the performance of fully fine-tuned models such as MedSAM and SAM-Med2D. Our SAM-TTA can also be seamlessly integrated into existing fine-tuned models, like MedSAM, to further boost their performance in medical image segmentation tasks.

**Limitation and Future Work.** Given that the adopted SAM only processes 2D images and many medical images (e.g., CT and MRI) are 3D, our method cannot process 3D data directly. Moreover, our approach relies on SAM’s pre-



trained representations. Therefore, if SAM exhibits limitations in certain medical imaging domains (for example, detecting very low-contrast lymph nodes in non-contrast CT scans), even test-time adaptation may yield only limited improvements. Future work will explore extending our framework to 3D medical image segmentation and integrating additional self-supervised cues to further enhance adaptation.

**Societal Impacts.** Our proposed SAM-TTA model may lead to inconsistent predictions in clinical applications since our design allows for multiple possible Bézier curves.

## References

- [1] Maruf Adewole, Jeffrey D Rudie, Anu Gbdamosi, Oluyemisi Toyobo, Confidence Raymond, Dong Zhang, Olubukola Omidiji, Rachel Akinola, Mohammad Abba Suwaid, Adaobi Emegoakor, et al. The brain tumor segmentation (brats) challenge 2023: Glioma segmentation in sub-saharan africa patient population (brats-africa). *arXiv preprint arXiv:2305.19369*, 2023. 5
- [2] Muhammad Awais, Muzammal Naseer, Salman Khan, Rao Muhammad Anwer, Hisham Cholakkal, Mubarak Shah, Ming-Hsuan Yang, and Fahad Shahbaz Khan. Foundation models defining a new era in vision: a survey and outlook. *IEEE Transactions on Pattern Analysis and Machine Intelligence*, 2025. 2
- [3] Cheng Chen, Juzheng Miao, Dufan Wu, Aoxiao Zhong, Zhiling Yan, Sekeun Kim, Jiang Hu, Zhengliang Liu, Lichao Sun, Xiang Li, et al. Ma-sam: Modality-agnostic sam adaptation for 3d medical image segmentation. *Medical Image Analysis*, 98:103310, 2024. 2
- [4] Tianrun Chen, Lanyun Zhu, Chaotao Ding, Runlong Cao, Shangzhan Zhang, Yan Wang, Zejian Li, Lingyun Sun, Papa Mao, and Ying Zang. Sam fails to segment anything?—sam-adapter: Adapting sam in underperformed scenes: Camouflage, shadow, and more. *arXiv preprint arXiv:2304.09148*, 2023. 1
- [5] Yizhou Chen, Xu-Hua Yang, Zihan Wei, Ali Asghar Heidari, Nenggan Zheng, Zhicheng Li, Huiling Chen, Haigen Hu, Qianwei Zhou, and Qiu Guan. Generative adversarial networks in medical image augmentation: a review. *Computers in Biology and Medicine*, 144:105382, 2022. 2
- [6] Ziyang Chen, Yongsheng Pan, Yiwen Ye, Mengkang Lu, and Yong Xia. Each test image deserves a specific prompt: Continual test-time adaptation for 2d medical image segmentation. In *CVPR*, pages 11184–11193, 2024. 3
- [7] Dongjie Cheng, Ziyuan Qin, Zekun Jiang, Shaoting Zhang, Qicheng Lao, and Kang Li. Sam on medical images: A comprehensive study on three prompt modes. *arXiv preprint arXiv:2305.00035*, 2023. 2
- [8] Junlong Cheng, Jin Ye, Zhongying Deng, Jianpin Chen, Tianbin Li, Haoyu Wang, Yanzhou Su, Ziyang Huang, Jilong Chen, Lei Jiang, et al. Sam-med2d. *arXiv preprint arXiv:2308.16184*, 2023. 2, 5, 6, 7
- [9] Junlong Cheng, Bin Fu, Jin Ye, Guoan Wang, Tianbin Li, Haoyu Wang, Ruoyu Li, He Yao, Junren Chen, JingWen Li, et al. Interactive medical image segmentation: A benchmark dataset and baseline. *arXiv preprint arXiv:2411.12814*, 2024. 2
- [10] Alexey Dosovitskiy, Lucas Beyer, Alexander Kolesnikov, Dirk Weissenborn, Xiaohua Zhai, Thomas Unterthiner, Mostafa Dehghani, Matthias Minderer, Georg Heigold, Sylvain Gelly, et al. An image is worth 16x16 words: Transformers for image recognition at scale. *arXiv preprint arXiv:2010.11929*, 2020. 5
- [11] Mark Everingham, SM Ali Eslami, Luc Van Gool, Christopher KI Williams, John Winn, and Andrew Zisserman. The pascal visual object classes challenge: A retrospective. *International Journal of Computer Vision*, 2015. 2
- [12] Ruochen Gao, Donghang Lyu, and Marius Staring. Swinlitemedsam: A lightweight box-based segment anything model for large-scale medical image datasets. In *Medical Image Segmentation Challenge*, pages 70–82. Springer, 2024. 2
- [13] David Gutman, Noel CF Codella, Emre Celebi, Brian Helba, Michael Marchetti, Nabin Mishra, and Allan Halpern. Skin lesion analysis toward melanoma detection: A challenge at the international symposium on biomedical imaging (isbi) 2016, hosted by the international skin imaging collaboration (isic). *arXiv preprint arXiv:1605.01397*, 2016. 5
- [14] Kaiming He, Xinlei Chen, Saining Xie, Yanghao Li, Piotr Dollár, and Ross Girshick. Masked autoencoders are scalable vision learners. In *CVPR*, 2022. 3
- [15] Edward J Hu, Yelong Shen, Phillip Wallis, Zeyuan Allen-Zhu, Yuanzhi Li, Shean Wang, Lu Wang, Weizhu Chen, et al. Lora: Low-rank adaptation of large language models. *ICLR*, 1(2):3, 2022. 4
- [16] Yuhao Huang, Xin Yang, Lian Liu, Han Zhou, Ao Chang, Xinrui Zhou, Rusi Chen, Junxuan Yu, Jiongquan Chen, Chaoyu Chen, et al. Segment anything model for medical images? *Medical Image Analysis*, 92:103061, 2024. 1
- [17] Debesh Jha, Pia H Smedsrud, Michael A Riegler, Pål Halvorsen, Thomas de Lange, Dag Johansen, and Håvard D Johansen. Kvasir-seg: A segmented polyp dataset. In *arXiv preprint arXiv:1911.07069*, 2019. 5
- [18] Neerav Karani, Ertunc Erdil, Krishna Chaitanya, and Ender Konukoglu. Test-time adaptable neural networks for robust medical image segmentation. *Medical Image Analysis*, 68: 101907, 2021. 3
- [19] Anahita Fathi Kazerooni, Nastaran Khalili, Xinyang Liu, Debanjan Haldar, Zhifan Jiang, Syed Muhammed Anwar, Jake Albrecht, Maruf Adewole, Udunna Anazodo, Hannah Anderson, et al. The brain tumor segmentation (brats) challenge 2023: focus on pediatrics (cbtnc-connect-dipgr-asnr-miccai brats-peds). *arXiv preprint arXiv:2404.15009*, 2024. 5
- [20] Amirhossein Kazerooni, Ehsan Khodapanah Aghdam, Moein Heidari, Reza Azad, Mohsen Fayyaz, Ilker Hacıhaliloglu, and Dorit Merhof. Diffusion models in medical imaging: A comprehensive survey. *Medical image analysis*, 88:102846, 2023. 2
- [21] Alexander Kirillov, Eric Mintun, Nikhila Ravi, Hanzi Mao, Chloe Rolland, Laura Gustafson, Tete Xiao, Spencer Whitehead, Alexander C Berg, Wan-Yen Lo, et al. Segment anything. In *ICCV*, pages 4015–4026, 2023. 1, 2, 3, 6, 7

- [22] Taha Koleilat, Hojat Asgariandehkordi, Hassan Rivaz, and Yiming Xiao. Medclip-sam: Bridging text and image towards universal medical image segmentation. In *MICCAI*, pages 643–653. Springer, 2024. 2
- [23] Jungsoo Lee, Debasmit Das, Jaegul Choo, and Sungha Choi. Towards open-set test-time adaptation utilizing the wisdom of crowds in entropy minimization. In *ICCV*, pages 16380–16389, 2023. 3
- [24] Mengqi Lei, Haochen Wu, Xinhua Lv, and Xin Wang. Condseg: A general medical image segmentation framework via contrast-driven feature enhancement. *arXiv preprint arXiv:2412.08345*, 2024. 2
- [25] Qing Li, Yizhe Zhang, Yan Li, Jun Lyu, Meng Liu, Longyu Sun, Mengting Sun, Qirong Li, Wenyue Mao, Xinran Wu, et al. An empirical study on the fairness of foundation models for multi-organ image segmentation. In *MICCAI*, pages 432–442. Springer, 2024. 2
- [26] Jian Liang, Ran He, and Tieniu Tan. A comprehensive survey on test-time adaptation under distribution shifts. *International Journal of Computer Vision*, 133(1):31–64, 2025. 3
- [27] Tsung-Yi Lin, Michael Maire, Serge Belongie, James Hays, Pietro Perona, Deva Ramanan, Piotr Dollár, and C Lawrence Zitnick. Microsoft coco: Common objects in context. In *ECCV*, 2014. 2
- [28] Jun Ma, Yuting He, Feifei Li, Lin Han, Chenyu You, and Bo Wang. Segment anything in medical images. *Nature Communications*, 15(1):654, 2024. 2, 5, 6, 7
- [29] Zachary Nado, Shreyas Padhy, D Sculley, Alexander D’Amour, Balaji Lakshminarayanan, and Jasper Snoek. Evaluating prediction-time batch normalization for robustness under covariate shift. *arXiv preprint arXiv:2006.10963*, 2020. 3
- [30] Maxime Oquab, Timothée Darcet, Théo Moutakanni, Huy Vo, Marc Szafraniec, Vasil Khalidov, Pierre Fernandez, Daniel Haziza, Francisco Massa, Alaaeldin El-Nouby, et al. Dinov2: Learning robust visual features without supervision. *arXiv preprint arXiv:2304.07193*, 2023. 2
- [31] Alec Radford, Jong Wook Kim, Chris Hallacy, Aditya Ramesh, Gabriel Goh, Sandhini Agarwal, Girish Sastry, Amanda Askell, Pamela Mishkin, Jack Clark, et al. Learning transferable visual models from natural language supervision. In *ICML*, 2021. 2
- [32] Yu Sun, Xiaolong Wang, Zhuang Liu, John Miller, Alexei Efros, and Moritz Hardt. Test-time training with self-supervision for generalization under distribution shifts. In *ICML*, pages 9229–9248. PMLR, 2020. 3
- [33] Antti Tarvainen and Harri Valpola. Mean teachers are better role models: Weight-averaged consistency targets improve semi-supervised deep learning results. *NeurIPS*, 30: 1195–1204, 2017. 5, 7
- [34] Jeya Maria Jose Valanarasu, Pengfei Guo, Vibashan VS, and Vishal M. Patel. On-the-fly test-time adaptation for medical image segmentation. In *MIDL*, pages 586–598. PMLR, 2024. 3
- [35] Dequan Wang, Evan Shelhamer, Shaoteng Liu, Bruno Olshausen, and Trevor Darrell. Tent: Fully test-time adaptation by entropy minimization. In *ICLR*, pages 1–12, 2021. 3, 5, 7
- [36] Qin Wang, Olga Fink, Luc Van Gool, and Dengxin Dai. Continual test-time domain adaptation. In *CVPR*, pages 7201–7211, 2022. 3, 5, 7
- [37] Wei Wang, Zhun Zhong, Weijie Wang, Xi Chen, Charles Ling, Boyu Wang, and Nicu Sebe. Dynamically instance-guided adaptation: A backward-free approach for test-time domain adaptive semantic segmentation. In *CVPR*, pages 24090–24099, 2023. 3
- [38] Ruxue Wen, Hangjie Yuan, Dong Ni, Wenbo Xiao, and Yaoyao Wu. From denoising training to test-time adaptation: Enhancing domain generalization for medical image segmentation. In *WACV*, pages 464–474, 2024. 3
- [39] Biao Wu, Yutong Xie, Zeyu Zhang, Jinchao Ge, Kaspar Yaxley, Suzan Bahadır, Qi Wu, Yifan Liu, and Minh-Son To. Bhsd: A 3d multi-class brain hemorrhage segmentation dataset. In *MLMI*, pages 147–156. Springer, 2023. 5, 6
- [40] Jianghao Wu, Ran Gu, Tao Lu, Shaoting Zhang, and Guotai Wang. UPL-TTA: Uncertainty-aware pseudo label guided fully test time adaptation for fetal brain segmentation. In *IPMI*, pages 237–249. Springer, 2023. 3, 5, 7
- [41] Junde Wu, Wei Ji, Yuanpei Liu, Huazhu Fu, Min Xu, Yanwu Xu, and Yueming Jin. Medical sam adapter: Adapting segment anything model for medical image segmentation. *arXiv preprint arXiv:2304.12620*, 2023. 1, 2
- [42] Yicheng Wu, Xiangde Luo, Zhe Xu, Xiaoqing Guo, Lie Ju, Zongyuan Ge, Wenjun Liao, and Jianfei Cai. Diversified and personalized multi-rater medical image segmentation. In *Proceedings of the IEEE/CVF Conference on Computer Vision and Pattern Recognition (CVPR)*, pages 11470–11479, 2024. 2
- [43] Longhui Yuan, Binhui Xie, and Shuang Li. Robust test-time adaptation in dynamic scenarios. In *CVPR*, pages 15922–15932, 2023. 3
- [44] Chunhui Zhang, Li Liu, Yawen Cui, Guanjie Huang, Weilin Lin, Yiqian Yang, and Yuehong Hu. A comprehensive survey on segment anything model for vision and beyond. *arXiv preprint arXiv:2305.08196*, 2023. 1
- [45] Haojie Zhang, Yongyi Su, Xun Xu, and Kui Jia. Improving the generalization of segmentation foundation model under distribution shift via weakly supervised adaptation. In *CVPR*, pages 23385–23395, 2024. 5, 7
- [46] Leying Zhang, Xiaokang Deng, and Yu Lu. Segment anything model (sam) for medical image segmentation: A preliminary review. In *BIBM*, pages 4187–4194. IEEE, 2023. 1
- [47] Shaoting Zhang and Dimitris Metaxas. On the challenges and perspectives of foundation models for medical image analysis. *Medical image analysis*, 91:102996, 2024. 2
- [48] Yichi Zhang, Zhenrong Shen, and Rushi Jiao. Segment anything model for medical image segmentation: Current applications and future directions. *Computers in Biology and Medicine*, page 108238, 2024. 1
- [49] Zongwei Zhou, Vatsal Sodha, Md Mahfuzur Rahman Siddiquee, Ruibin Feng, Nima Tajbakhsh, Michael B Gotway, and Jianming Liang. Models genesis: Generic autodidactic models for 3d medical image analysis. In *MICCAI*, pages 384–393. Springer, 2019. 3